

## Process Intensification of Mesoporous Material's Synthesis by Microwave-Assisted Surfactant Removal

López-Pérez, Lidia; López-Martínez, Marco Antonio; Djanashvili, Kristina; Góra-Marek, Kinga; Tarach, Karolina A.; Borges, María Emma; Melián-Cabrera, Ignacio

**DOI**

[10.1021/acssuschemeng.0c05438](https://doi.org/10.1021/acssuschemeng.0c05438)

**Publication date**

2020

**Document Version**

Accepted author manuscript

**Published in**

ACS Sustainable Chemistry and Engineering

**Citation (APA)**

López-Pérez, L., López-Martínez, M. A., Djanashvili, K., Góra-Marek, K., Tarach, K. A., Borges, M. E., & Melián-Cabrera, I. (2020). Process Intensification of Mesoporous Material's Synthesis by Microwave-Assisted Surfactant Removal. *ACS Sustainable Chemistry and Engineering*, 8(45), 16814-16822. <https://doi.org/10.1021/acssuschemeng.0c05438>

**Important note**

To cite this publication, please use the final published version (if applicable). Please check the document version above.

**Copyright**

Other than for strictly personal use, it is not permitted to download, forward or distribute the text or part of it, without the consent of the author(s) and/or copyright holder(s), unless the work is under an open content license such as Creative Commons.

**Takedown policy**

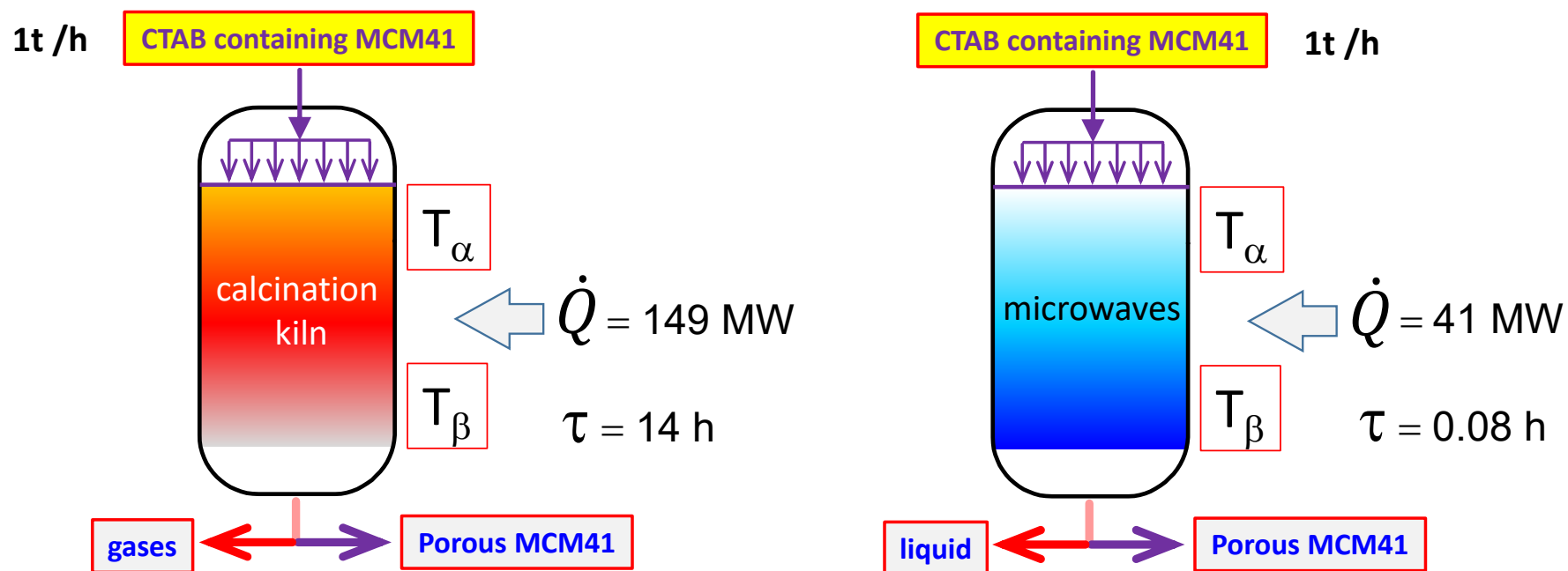
Please contact us and provide details if you believe this document breaches copyrights. We will remove access to the work immediately and investigate your claim.

This document is confidential and is proprietary to the American Chemical Society and its authors. Do not copy or disclose without written permission. If you have received this item in error, notify the sender and delete all copies.

### Process Intensification of Mesoporous Material's Synthesis by Microwaves-assisted Surfactant Removal

Journal:	<i>ACS Sustainable Chemistry &amp; Engineering</i>
Manuscript ID	sc-2020-05438g.R1
Manuscript Type:	Article
Date Submitted by the Author:	n/a
Complete List of Authors:	Lopez-Perez, Lidia; Universidad Autonoma Metropolitana Azcapotzalco, Ciencias Básicas Lopez Martinez, Marco Antonio; Universidad Autonoma Metropolitana Azcapotzalco, CIENCIAS BASICAS Djanashvili, Kristina; Technische Universiteit Delft, Department of Biotechnology Góra-Marek, Kinga; Uniwersytet Jagiellonski w Krakowie, Department of Chemistry Tarach, Karolina; Uniwersytet Jagiellonski w Krakowie, Faculty of Chemistry Borges, Emma; University of La Laguna, Chemical Engineering & P.T. Melian Cabrera, Ignacio; University of La Laguna, Chemical Engineering & P.T.

SCHOLARONE™  
Manuscripts



1  
2  
3  
4  
5  
6  
7  
8  
9  
10  
11  
12  
13  
14  
15  
16  
17  
18  
19  
20  
21  
22  
23  
24  
25  
26  
27  
28  
29  
30  
31  
32  
33  
34  
35  
36  
37  
38  
39  
40  
41  
42  
43  
44  
45  
46  
47  
48  
49  
50  
51  
52  
53  
54  
55  
56  
57  
58  
59  
60

# Process Intensification of Mesoporous Material's Synthesis by Microwaves-assisted Surfactant Removal

Lidia López-Pérez,<sup>1,2§</sup> Marco-Antonio López-Martínez,<sup>2,§</sup> Kristina Djanashvili,<sup>3</sup>

Kinga Góra-Marek,<sup>4</sup> Karolina Tarach,<sup>4</sup> Emma Borges<sup>5</sup>

and Ignacio Melián-Cabrera<sup>5,\*</sup>

1. Faculty of Science and Engineering, University of Groningen, Nijenborgh 4, 9747 AG Groningen, The Netherlands.

2. División de Ciencias Básicas e Ingeniería, Universidad Autónoma Metropolitana- Unidad Azcapotzalco, Av. San Pablo 180, Col. Reynosa Tamaulipas, Alc. Azcapotzalco 02200, Mexico City, Mexico.

3. Department of Biotechnology, Delft University of Technology, Van der Maasweg 9, 2629HZ Delft, The Netherlands.

4. Faculty of Chemistry, Jagiellonian University in Kraków, 2 Gronostajowa St., 30-387 Kraków, Poland.

5. Chemical Engineering Department, University of La Laguna, Avda. Astrofísico Francisco Sánchez, s/n. Faculty of Science, PO BOX 456, 38200 San Cristóbal de La Laguna, S/C de Tenerife, Spain.

§ Authors contributed equally

Corresponding author:

E: [ignacio.melian.cabrera@ull.edu.es](mailto:ignacio.melian.cabrera@ull.edu.es)

**Abstract**

Mesoporous materials are of vital importance for uses in separation, adsorption and catalysis. The first step in their preparation consists of synthesising an organic-inorganic hybrid in which a structuring directing agent (SDA, normally a surfactant) is used to provide the desired porosity. The most common method to eliminate the SDA, and generate the porosity, is high-temperature calcination. Such a process is energy-intensive and slow. In this study, we investigated alternative non-thermal surfactant removal methods on a soft MCM-41 material, aiming at reducing the processing time and temperature, whereas maximizing the material's properties. The choice of a soft MCM-41 is critical since it is hydrothermally unstable, where the SDA removal is troublesome. Microwave processing yielded outstanding performance in terms of surfactant removal, structural preservation and textural features; the surfactant was fully removed, the hexagonal structure was preserved and the surface was highly rich in Si-OH groups. It is suggested that H<sub>2</sub>O<sub>2</sub> is the dominant oxidant. In terms of the process features, the processing time is significantly reduced, 14h (calcination) versus 5 min (microwaves), and the applied temperature is much lower. The energy savings were estimated to be 72% lower as compared to calcination; therefore, this approach contributes to the process intensification of a very relevant material's production.

**KEYWORDS:** Microwaves-assisted processing; structured mesoporous material; energy-saving processing; structural preservation; mild SDA removal; quick-processing; H<sub>2</sub>O<sub>2</sub> oxidation

## Introduction

Mesoporous materials are highly-sophisticated nano-structures with application in catalysis, adsorption, sensing and separation, to cite a few. They are considered applied functional nano-materials.<sup>1-3</sup> As compared to zeolites that are microporous solids (*i.e.* pores with diameters less than 2 nm),<sup>4</sup> mesoporous materials expand the pore-size and overcome the limitations of zeolite networks. This allows a smoother and unrestricted diffusion of bulkier molecules, and even lineal polymers can penetrate and be converted.<sup>5</sup> In order to obtain such a control in the pore size at nano-scale, an entirely-new strategy was developed by using supramolecular organic molecules as structuring directing agents (SDA) in the sol-gel. Those templates can range from cationic, anionic and non-ionic (neutral) surfactants, normally leading to mesoporous materials,<sup>1,6</sup> though macroporosity can also be obtained.<sup>7,8</sup>

Mesoporous materials can range in the structure from hexagonal such as MCM-41 (a member of the M41S family),<sup>9,10</sup> SBA-15<sup>11,12</sup> and SBA-3;<sup>13</sup> cubic such as MCM-48,<sup>14</sup> FDU-5<sup>15</sup> and AMS-10;<sup>16</sup> caged structures such as SBA-2,<sup>17</sup> FDU-1,<sup>18</sup> SBA-1,<sup>19</sup> deformed mesophases such as SBA-8,<sup>20</sup> KSW-2;<sup>21</sup> and low-order mesophases such as KIT,<sup>22</sup> HMS<sup>23</sup> and MSU-*n*.<sup>24</sup> Though the composition is generally based on silica, other non-silica compositions include alumina,<sup>25,27</sup> or wider compositions such as CeO<sub>2</sub>, MoO<sub>3</sub>, WO<sub>3</sub>, CeO<sub>2</sub>-ZrO<sub>2</sub>, α-Fe<sub>2</sub>O<sub>3</sub>, WO<sub>3</sub>-TiO<sub>2</sub> and TiO<sub>2</sub>.<sup>28-30</sup> The addition of elements in smaller quantity into the main phase, *e.g.* alumina-containing silicates, makes the spectral composition nearly infinite for mesoporous materials.

The surface and pore properties of the mesoporous materials are of great importance for application. The first step in their manufacturing consists of obtaining the ordered non-porous organic-inorganic hybrid, in which the SDA (or surfactant) is occupying the pores. The next delicate step is to extract the surfactant from the cavities to develop the porosity, without

1  
2  
3 influencing the original structure, or altering the properties minimally. The SDA removal is  
4  
5 therefore decisive on the final properties. Specifically, the SDA removal's method has to be  
6  
7 wisely adjusted as a function of the stability of the network, desired properties (*e.g.* surface  
8  
9 chemistry), and implementation features.  
10

11  
12 Calcination consists of a thermal treatment of the solid. By increasing the temperature up to  
13  
14 550 °C, the SDA present in the pores will decompose and finally burn out into CO<sub>2</sub> and H<sub>2</sub>O.  
15  
16

17 The stability upon calcination is a function of the wall thickness between the pores. However,  
18  
19 a shrinkage of the unit cell is always observed.<sup>31</sup> The silanol groups, Si(OSi)<sub>3</sub>OH, combine to  
20  
21 produce water and new siloxane bonds are formed, which results in structural shrinkage.<sup>10,32</sup>  
22  
23

24 The formation of siloxane units can influence the surface properties, such as hydrophilicity  
25  
26 and acidity. Hence, changes in the concentration of surface –OH groups induce variations in  
27  
28 the surface hydrophilic/hydrophobic character. This can affect the adsorption of reagents  
29  
30 both in the number of adducts formed and their nature. In order to minimize the calcination  
31  
32 side effects, different approaches have been suggested.<sup>33-35</sup> However, controlling the surface  
33  
34 chemistry is still a challenging target.  
35  
36  
37

38  
39 Mesoporous materials of high interest are those that are synthesised in simple manners,  
40  
41 which often implies free of hydrothermal treatment.<sup>36</sup> But that brings the drawback that these  
42  
43 structures are soft and prone to damage in successive processing steps. The primary goal of  
44  
45 this work was to identify a suitable method to remove the SDA of a soft MCM-41 material,  
46  
47 aiming at a process that reduces the processing time, decrease the energy consumption and  
48  
49 the material's properties are maximised. Therefore, we were looking at an intensified process  
50  
51 for a mild non-thermal SDA removal of a relevant MCM-41 material. The methodology  
52  
53 reported by Tian *et al.*<sup>37</sup> using microwaves is attractive, which was applied on an SBA-15.  
54  
55  
56  
57

1  
2  
3 However, applying such a methodology onto an MCM-41 is not a rational choice since the  
4 materials' hydrothermal stability are very different; SBA-15 is hydrothermally stable whereas  
5 the studied MCM-41 is not. Therefore, this work gives more value to the microwave  
6 processing, since it expands its application range into hydrothermally unstable materials. Most  
7 importantly, this work provides original aspects from the process point of view, in terms of  
8 significant energy reduction through the microwaves processing.  
9  
10  
11  
12  
13  
14  
15  
16  
17

## 18 **Experimental**

### 19 **Chemicals**

20  
21 The employed chemicals are summarised in the Table S1, Electronic Supporting Information.  
22  
23  
24  
25

### 26 **Synthesis of the mesophase**

27  
28 The MCM-41 mesophase was prepared at room temperature following the procedure  
29 reported by Grün *et.al.*<sup>36</sup> A solution containing the quaternary ammonium salt (CTAB, as  
30 structuring directing agent) in Milli-Q water was prepared under gentle magnetic stirring.  
31 Aqueous ammonia was added to the solution as a catalyst. Then, TEOS was added dropwise.  
32  
33 During the addition of TEOS, the mixture began to whiten resulting in a gel with the following  
34 molar composition: 1 TEOS: 0.152 CTAB: 2.8NH<sub>3</sub>: 141.2 H<sub>2</sub>O. The mixture was stirred for one  
35 hour. The precipitate was recovered by suction filtration and washed with abundant water. A  
36 fine white powder was obtained after drying overnight at 90 °C. Note that the terms SDA and  
37 surfactant are equally used along the manuscript; they are equivalent terms.  
38  
39  
40  
41  
42  
43  
44  
45  
46  
47  
48  
49  
50  
51  
52  
53  
54  
55  
56  
57  
58  
59  
60

### SDA removal methodologies

Calcination. A ceramic cup, which contained the sample, was placed in the centre of a box Nabertherm furnace, equipped with P330 temperature controller, and heated from room temperature up to 550 °C for 5 h in the presence of static air. The heating rate was 1 °C/min.

Solvent-extraction. The method consisted of contacting the solid with an acidic ethanol solution at the reflux temperature. One gram of the mesophase was contacted with 300 mL of a 1.0 M HCl solution in ethanol. The mixture was stirred and kept in reflux for 30 h at the reflux temperature (~78 °C). The sample was filtered and washed with abundant water and dried in an oven at 110 °C.

Ozonation. The treatment with ozone was performed according to the procedure reported by Büchel *et al.*<sup>38</sup> The method consists of bubbling *in-situ* produced ozone through a mixture of the material and water. Typically, 1 g of the precursor material was contacted with 150 mL of Milli-Q water and agitated with a magnetic stirrer. Ozone was then introduced to the slurry by bubbling the gas through a glass tube. At the beginning of the reaction, the hydrophobic powder (mesophase containing the template) did not mix well in water and remained on top of the liquid surface. After approx. 30 min, the slurry resulted in a homogeneous suspension. The experiment was stopped after 8h; the slurry was filtered, washed with abundant water by filtration and dried in an oven at 110 °C.

Microwave-assisted template removal. A microwave sample preparation system MDS 2000 (CEM Corporation) was used, that is equipped with Teflon sample vessels transparent for microwave radiation. The working frequency and voltage of the equipment were 2450 MHz and 220V, respectively. The samples were prepared in the Teflon vessel using 0.15 g of mesophase combined with 1.5 mL of HNO<sub>3</sub> solution and 1.0 mL of H<sub>2</sub>O<sub>2</sub> (see concentrations in

1  
2  
3 Electronic Supporting Information, Table S1), using a modified protocol as reported  
4  
5 elsewhere.<sup>37</sup> The maximum observed temperature was 200 °C. The mesophase was first  
6  
7 exposed to different treatment times to determine the time needed to fully remove the  
8  
9 template. Preliminary experiments were done for 3, 5 and 7 minutes. A processing time of 5  
10  
11 min was found to be necessary to achieve full SDA removal. The slurry was filtered, washed  
12  
13 with abundant water by filtration and dried in an oven at 110 °C.  
14  
15

16  
17 Fenton-assisted SDA removal. This protocol was carried out following the protocol described  
18  
19 by López-Pérez *et al.*<sup>10</sup> in liquid-phase without the need of any solvent.  
20  
21

## 22 **Characterisation methods**

23  
24  
25 Elemental analysis. CHN elemental analysis was carried out on a EuroVector 3000 CHNS  
26  
27 analyser, using approximately 2 mg-sample, which was weighted on a 6-digit Mettler-Toledo  
28  
29 analytical scale. The analyses were done in duplicate and only analyses with a 2% standard  
30  
31 deviation were employed. The analysis itself consists of burning the samples at 1700-1800 °C  
32  
33 in the presence of an oxidation catalyst. The organics are decomposed into CO<sub>2</sub>, H<sub>2</sub>O, SO<sub>2</sub> and  
34  
35 N<sub>2</sub> and then separated via an online gas chromatograph having a Poropak QS column,  
36  
37 operated isothermally at 80 °C, and quantified with a thermal conductivity detector.  
38  
39 Calladius™ software was used to obtain the quantitative information. The integrated peak  
40  
41 height was converted into a percentage, using acetanilide (99.9%) as an external standard.  
42  
43  
44

45  
46 Structure. The structural ordering was evaluated by small-angle X-ray scattering (SAXS) on a  
47  
48 Bruker NanoStar instrument, containing a ceramic fine-focus X-ray tube, which was powered  
49  
50 by a Kristallflex K760 generator at 35 kV and 40 mA. The X-ray flux was collimated using cross-  
51  
52 coupled Göbel mirrors and a 0.1 mm-diameter pinhole, providing a CuK $\alpha$  beam with a full  
53  
54 width at half-maximum of about 0.2 mm at the sample position. The sample-to-detector  
55  
56  
57

1  
2  
3 distance was 1.04 m. The scattering intensity was registered by a Siemens AXS Hi-Star detector  
4  
5 in the q-vector range of 0.1–2.0 nm.  
6

7 Gas adsorption. Nitrogen adsorption isotherms at –196 °C were obtained on a QuantaChrome  
8  
9 Autosorb-6B apparatus. The materials were previously evacuated at 150 °C for 16 h. The BET  
10  
11 (Brunauer–Emmett–Teller) method was used to calculate the surface area ( $S_{\text{BET}}$ ) of the  
12  
13 samples. The BJH (Barrett–Joyner–Halenda) method was applied for deriving the pore size  
14  
15 distributions of the solids. The total pore volume was estimated from the amount adsorbed  
16  
17 at a relative pressure of 0.98 in the desorption branch.  
18  
19

20  
21 Thermal analysis. Thermogravimetric analyses were carried out in a TGA/SDTA851e Mettler–  
22  
23 Toledo analyser, where around 5 to 10 mg of sample was loaded into a 70  $\mu\text{L}$   $\alpha\text{-Al}_2\text{O}_3$  crucible.  
24  
25 The temperature was raised from 30 to 900 °C at a rate of 10 °C/min under a flow of synthetic  
26  
27 air (100 mL/min). Baseline subtraction was employed to remove geometrical and crucible  
28  
29 effects in the pattern.  
30  
31

32  
33 Scanning electron imaging. SEM images were recorded with a Philips XL 20 microscope at 10  
34  
35 kV. Samples were coated with gold to improve contrast.  
36

37 High-resolution transmission electron imaging. TEM micrographs were recorded on a JEOL  
38  
39 2010. A small amount of sample was grinded with a mortar and pestle and dispersed in  
40  
41 isopropanol. A small drop was dispersed on a Holey carbon grid (TED Pella 300 Copper Mesh)  
42  
43 and left to dry. Images were taken at 200 kV in brightfield and analysed using the software  
44  
45 Gatan Digital Micrograph.  
46  
47

48 DRIFTS. The IR spectra of the materials were collected on a Nicolet Magna 860 spectrometer,  
49  
50 equipped with a DTGS detector. The spectra were acquired by co-addition of 256 scans with  
51  
52 a resolution of 4  $\text{cm}^{-1}$ . About 50 mg of the pure material was packed into a sample holder and  
53  
54 synthetic air was passed over the sample and the material was mildly dried at 150 °C until the  
55  
56  
57

1  
2  
3 baseline of the  $m/z=18$  ( $H_2O$ ) of the outlet gas stream went to a baseline level, indicating that  
4  
5 the physisorbed water was removed from the sample's surface. A DRIFT spectrum of dried KBr  
6  
7 (Aldrich, FTIR grade) was first recorded as a background.  
8

9  
10 Solid state NMR.  $^{29}Si$  MAS NMR spectra were measured on a Varian VXR-400S spectrometer  
11  
12 at 79.44 MHz using a 7-mm zirconium spinner, with the following settings: spinning speed 5  
13  
14 KHz, acquisition time 0.2 s, acquisition delay 20 s, radiofrequency length 3.2  $\mu s$ , spectral  
15  
16 window 30007 Hz and 3200 scans. Tetramethylsilane (TMS) was used as reference.  
17  
18

## 19 20 21 22 **Results and Discussion**

### 23 24 25 **Mesophase**

26  
27  
28 The mesophase was prepared according to Grün *et al.*<sup>36</sup> SAXS analysis reveals a mesophase  
29  
30 having well-defined hexagonally packed cylindrical morphology characterised by a distance  
31  
32 between the cylinders of 4.76 nm (Figure 1A), which was confirmed by high-resolution TEM  
33  
34 (Figure 1B). SEM provided information on the particle morphology, displaying agglomerates  
35  
36 of particles that are mostly unconnected of relatively small size,  $\sim 0.5 \times 2 \mu m$  (Figure S1 in ESI).  
37  
38 Thermogravimetric analysis (Figure 1C) indicates that the mesophase requires a thermal  
39  
40 treatment of 550 °C to decompose the SDA (*i.e.* CTAB surfactant). The surfactant is present in  
41  
42 42 wt.% and decomposes in two steps in agreement with prior studies, DTGA in Fig. 1C.<sup>39,40</sup>  
43  
44  
45  
46

### 47 48 **Calcination**

49  
50  
51 As discussed earlier in the background, calcination may produce a structural shrinkage. This is  
52  
53 shown in Figure 2A, where the main (100) reflection shifts to higher angles. The hexagonal  $a_0$   
54  
55 lattice parameter changes from 4.76 down to 4.28 nm, representing 10% contraction. The  
56  
57

1  
2  
3 contraction of the structure is not a big problem for catalysis purposes, but the main drawback  
4  
5 of calcination refers to the fact that it irreversibly reduces the density of surface OH groups  
6  
7 and, from the practical point of view, it is a slow and an energy-intensive process.  
8  
9

## 10 **Non-thermal SDA removal methodologies**

11  
12  
13 After performing mild SDA removal protocols on the mesophase, the resulting materials were  
14  
15 characterised by several techniques to assess template removal and the materials' properties.  
16  
17

18  
19 **Surfactant removal efficiency.** Thermogravimetric analysis gave ambiguous information as  
20  
21 the mildly-treated materials have a significant weight loss due to dehydroxylation's water  
22  
23 release. CHN analysis is selective and can provide a straight account of the SDA removal.  
24  
25 Therefore, the template removal efficiency was obtained after comparing the elemental  
26  
27 composition (CHN analysis) before and after each procedure (Table 1). Besides calcination that  
28  
29 removes all the SDA, microwave oxidation and Fenton are the most effective alternatives to  
30  
31 calcination. High SDA removal was also obtained by solvent extraction. Ozonation does not  
32  
33 provide good results with an SDA removal efficiency of 29% only. These results were compared  
34  
35 with DRIFTS (Figure 2B). Inspection of the 2840-3000  $\text{cm}^{-1}$  C-H region confirms that the SDA  
36  
37 removal is complete for the microwaved material, being as efficient as calcination. As a  
38  
39 reference case, the ozone treatment shows a substantial contribution of C-H groups  
40  
41 originating from the undecomposed SDA.  
42  
43  
44  
45  
46

47 **Structural ordering.** Small-angle X-ray diffraction patterns provide information about the  
48  
49 structural changes upon each SDA removal strategy (Figure 3A). Structural shrinkage is  
50  
51 detected for all the materials. The main Bragg diffraction peak (100) is shifted to higher values  
52  
53 that results in smaller cell parameters ( $a_0$ , Table 1). The larger degree of shrinkage took place  
54  
55  
56  
57

1  
2  
3 upon calcination (~10%). Shrinkage was also observed upon microwave oxidation (~6%). The  
4  
5 temperatures achieved during microwave radiation (~200 °C) and the presence of H<sub>3</sub>O<sup>+</sup>  
6  
7 (H<sub>5</sub>O<sub>2</sub><sup>+</sup>) in an aqueous environment, may explain the structural shrinkage. Such a shrinkage  
8  
9 was also found, but to a lower extent, in the ozonation and Fenton treatments (4 and 2%,  
10  
11 respectively). The reason for shrinkage in these cases appears to be related to hydrolysis of  
12  
13 the soft un-calcined silica framework. This is supported by the conclusions of López-Pérez *et*  
14  
15 *al.*,<sup>10</sup> who showed that a 70 °C-Fenton treatment leads to severe structural collapse on an  
16  
17 MCM-41 mesophase. This was explained by the high capillary forces during the drying of the  
18  
19 pores; similar observations were found for an SBA-15, associated to the soft nature of the  
20  
21 silica network as well.<sup>12</sup>  
22  
23  
24  
25

26 Changes in the mesoscopic ordering were observed by comparing the SAXS patterns in Figure  
27  
28 3A. Calcination shows the highest degree of ordering, followed by microwaving with a less  
29  
30 intense and broader (100) reflection. The second-order reflections of this material are also  
31  
32 less intense; hence the material's contraction is isotropic (*i.e.*  $x \sim y \sim z$ ). The Fenton treatment  
33  
34 only presented an ill-defined (100) peak; while the secondary ones were undetected. The  
35  
36 structures with the lowest ordering correspond to the ozone-treated followed by the solvent  
37  
38 extraction; in the latter case, no pattern was detected. The materials which were exposed to  
39  
40 an aqueous environment for prolonged periods of time resulted in structural collapse, most  
41  
42 likely due to hydrolysis. Control tests were carried out to verify that hypothesis. The calcined  
43  
44 MCM-41 was hydrothermally treated at 70 °C mirroring those treatments. From these  
45  
46 experiments, it became evident that the hydrothermal treatment leads to severe structural  
47  
48 and textural modifications, as evidenced from SAXS patterns (Figure 4A) and the isotherms  
49  
50 (Figure 4B, textural parameters can be found in Table S-3 in ESI). Even after 1h, the structure  
51  
52 fully collapses with a severe drop in the textural parameters (Table S3 in ESI). These results  
53  
54  
55  
56  
57  
58  
59  
60

confirm the susceptibility of this mesophase towards hydrothermal treatments, due to hydrolysis.

**Textural features.** The textural properties were studied by gas adsorption. The nitrogen isotherms (Figure 3B) show type IV isotherms for the calcined and microwaves-processed materials. Calcination of the mesophase gives rise to a well-defined porosity with a fully-reversible adsorption isotherm. It has a specific surface area of 1077 m<sup>2</sup>/g and a pore volume of 0.85 cm<sup>3</sup>/g. The porosity of the other materials is affected by alterations and/or damage in the structure. The microwaved material is the one which still shows a high adsorption capacity with a moderate modification in the pore-filling mechanism. It is not as sharp as in the calcined case, and it occurs in two steps. The other materials do not show a steep pore-filling step, but it is nearly flat in the typical mesopore region; they possess lower surface areas and pore volumes (Table 1).

The BJH pore size distributions (Figure 3C) are in agreement with the SAXS ordering. Only the calcined material has a well-resolved BJH pore size distribution (PSD) at around 2.6 nm. The microwaved material has a broader pattern with the prevalence of pore sizes at *ca.* 2.6 nm. The pore maximum at high  $P/P_0$  is due to a phenomenon called tensile strength effect (TSE in Figure 3C).<sup>41</sup> Despite having the TSE effect, the PSD of the microwaved material shows evidence of having broader pores; this was verified by estimating the average pore size as  $4 \cdot 10^3 \times \frac{V_{total}}{S_{BET}}$ , which resulted in 3.2 nm for the calcined and 3.6 nm for the microwaved one. Note that it is known that the BJH model gives an underestimation of the pore size when comparing BJH with geometrical pore size values.<sup>42</sup> The other materials displayed a PSD with a baseline-like pattern. Despite the microwave approach modified the PSD with secondary larger pores, this did not have a big effect in the textural parameters. The BET surface area and pore volume

1  
2  
3 remain high with 923 m<sup>2</sup>/g and a pore volume of 0.82 cm<sup>3</sup>/g. This is 85% and 96% of the BET  
4  
5 and pore volume retention, as compared to calcination. The drop in the BET is due to having  
6  
7 bigger pores.  
8

9  
10 The broader PSD of the microwaved material was further investigated by high-resolution TEM  
11 (Figure 5A). It was found that the material was in general ordered but some domains were  
12  
13 more amorphous indicating the disturbance of the regularity. This is ascribed to hydrolysis,  
14  
15 which makes the structure more disordered. The combination of water and local hot-spots  
16  
17 originated from the microwave beam, can alter local parts of the material. Such an effect was  
18  
19 absent in the calcined material (Figure 5B) where a regular distribution of pores/channels was  
20  
21 observed across the particle.  
22  
23  
24  
25

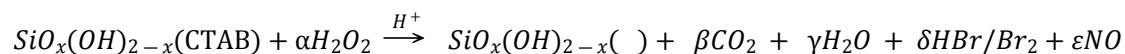
26  
27 To understand better the PSD broadening, one must bear in mind that the microwaves-  
28  
29 processing functions like a batch autoclave where the pressure increases above 1 MPa and  
30  
31 temperatures at around 200 °C. That means that such a treatment can act as a secondary  
32  
33 hydrothermal step on the structure. It was generally found for SBA-15 materials that the pore  
34  
35 size increases with the hydrothermal temperature during the hydrothermal ageing;<sup>33</sup> a similar  
36  
37 effect may be occurring here where the pore size is expanded due to the microwaves-induced  
38  
39 heat and autogenous pressure. However, it is not yet entirely clear if the effect in this situation  
40  
41 is local or not (*i.e.* affecting the whole sample or a section), since the TEM images did not have  
42  
43 enough resolution in the range of the observed pore sizes, 2 to 4 nm, to identify the pore  
44  
45 broadening. In practical terms, the pore expansion may be resolved, or minimised, by novel  
46  
47 reactor concepts with controlled doses of microwaves, spinning, etc. as will be outlined later.  
48  
49  
50  
51 Therefore, this approach can still be considered as suboptimal, at this stage.  
52  
53  
54  
55  
56  
57  
58  
59  
60

1  
2  
3 **Silanol characterisation.** The properties of the resulting material in terms of the silanol groups  
4  
5 were studied by DRIFTS and  $^{29}\text{Si}$  MAS NMR. Several kinds of silanol groups can be distinguished  
6  
7 in the IR spectra (Figure 6A). Freely oscillating isolated terminal  $(\text{SiO})_3\text{Si-OH}$  were found at  
8  
9  $3750\text{ cm}^{-1}$ . The broad band at  $3540\text{ cm}^{-1}$  is typical of strongly linked silanols as vicinal  
10  
11 hydrogen-bonded silanols (dimers or higher).<sup>43</sup> It is well seen that the microwaved treatment  
12  
13 results in a *ca.* two-fold higher number of hydrogen-bonded silanols (higher intensity of the  
14  
15  $3540\text{ cm}^{-1}$  band). This suggests that the microwave treatment does not condense the silanols  
16  
17 as calcination does, and it may contain surface defects where the OH-linked silanols are  
18  
19 located. The concentration of the hydrogen-bonded silanols normally decreases by increasing  
20  
21 the pore size,<sup>44</sup> but this is not observed for the microwaved material despite having broader  
22  
23 pores, which is a positive feature.

24  
25  
26  
27  
28  $^{29}\text{Si}$  MAS NMR completes the interpretation of the surface chemistry (Figure 6B). The  $\text{Q}_2$   
29  
30 ( $\text{Si}(\text{OSi})_2(\text{HO})_2$ , geminal) and  $\text{Q}_3$  ( $\text{Si}(\text{OSi})_3(\text{HO})$ , isolated and vicinal terminal) are more  
31  
32 pronounced in the microwaved material. This corresponds to the presence of a highly  
33  
34 hydroxylated surface. The concentration of Si-OH was quantified (Table 2), resulting in  
35  
36 comparable values between the microwave-processed MCM-41 and the starting mesophase,  
37  
38 whereas the calcined counterpart lost 19%. The high Si-OH in the microwaved material has to  
39  
40 do with the mild conditions; there is no thermal condensation of Si-OH into siloxane. This  
41  
42 explains that the mesophase and the microwaves-processed materials have a comparable Si-  
43  
44 OH concentration. The highly hydroxylated surface's nature of the microwaved material can  
45  
46 also be seen in the  $\text{Q}_4$  ( $\text{Si}(\text{OSi})_4$ ) NMR's peak. The upfield shift of the resonance towards the  
47  
48 negative edge suggests the removal of a less electronegative element from the Si local  
49  
50 environment. This indicates the engagement of H from an OH group in the hydrogen-bond  
51  
52 with a neighbouring O-atom from the silanols.

1  
2  
3 In practical terms, having a high amount of silanols (not Si-O-Si units) makes the microwaves-  
4  
5 processed material more hydrophilic, opening doors of adsorption strategies for *e.g.* improved  
6  
7 drug load,<sup>45</sup> or grafting procedures where the high concentration of silanols would be needed.  
8  
9 Figure 6A (inset) represents a section of the pore displaying a high density of Si-OH; in this  
10  
11 case, for simplicity, the vicinal ones have been represented.  
12  
13

14  
15 **Mechanistic considerations for the microwaves-processing method.** When comparing the  
16  
17 oxidation potentials between the two employed oxidants, it is thought that the prevalent  
18  
19 oxidizing agent is H<sub>2</sub>O<sub>2</sub> (1.776 V)<sup>46</sup> while HNO<sub>3</sub> (0.803-0.934 V)<sup>46</sup> can only have an acidifying  
20  
21 role. This opens up the possibility to optimise the process by reducing the use of HNO<sub>3</sub> in a  
22  
23 successive study. Though Fenton radicals (2.800 V)<sup>47</sup> are stronger in terms of oxidation  
24  
25 potential than H<sub>2</sub>O<sub>2</sub>, the benefit of the microwaves is the fact that the temperature increases  
26  
27 up to 200 °C; this favours the SDA oxidation kinetics using H<sub>2</sub>O<sub>2</sub>. Under ambient conditions,  
28  
29 Fenton chemistry would be better since the maximum temperature is given by the H<sub>2</sub>O<sub>2</sub>/H<sub>2</sub>O  
30  
31 mixture's boiling temperature, *ca.* 100 °C; at these conditions, H<sub>2</sub>O<sub>2</sub> cannot compete in kinetic  
32  
33 terms with Fenton chemistry. However, as seen in the materials properties, Fenton does not  
34  
35 work well for this material since it leads to severe structural and textural collapse. In other  
36  
37 words, the microwaves-induced autoclaving effect promotes the oxidation kinetics of H<sub>2</sub>O<sub>2</sub>  
38  
39 and makes it an effective oxidant for the CTAB oxidation. A tentative mechanism for the SDA  
40  
41 removal can be defined as:  
42  
43  
44  
45  
46  
47



49  
50  
51 Where CTAB is decomposed into CO<sub>2</sub>, H<sub>2</sub>O, HBr/Br<sub>2</sub> and NO. SiO<sub>x</sub>(OH)<sub>2-x</sub>( ) represents the SDA-  
52  
53 free MCM-41 material, containing siloxanes and silanols.  
54  
55  
56  
57  
58  
59  
60

## Methodologies' evaluation

It is outstanding that the majority of materials underwent structural damage upon the different SDA removal methodologies. This supports the fact that the mesophase, without hydrothermal treatment, does not have an adequate hydrothermal stability. The success of the microwave treatment in keeping the structure is associated to the short treatment times (minutes); this enables the SDA removal and minimizes the structural damage.

A comparison of the protocols' properties is given in Table 3. Most of the methodologies are effective in removing the SDA (rated as ++), except ozonation (+). The SDA removal approach utterly affects the ordering leading to less ordered (+/-) or amorphous (-) structures, with the exception of calcination (++) and microwave treatment (+). The ordering is directly linked to the porosity; those materials with higher ordering display better textural parameters. The evaluation also considers process features. Calcination is slow due to the low heating rates, with a total processing time of ~14h. The corrosive gasses can affect irreversibly the calcination equipment, leading to a long return on investment (*i.e.* recapitalisation) and it is highly energy-intensive. Microwave is a much faster protocol and operates at a lower temperature. The Fenton chemistry-derived material would be improved by drying using a low-surface tension solvent, as proven by López-Pérez et al.,<sup>10</sup> in the sense that the structure was much better preserved when H<sub>2</sub>O was replaced by *n*-BuOH during the drying. This avoids surface tension-induced collapse. However, such *n*-BuOH post-treatment notably increases the complexity of the work-up, whereas the microwaves processing seems to overcome such problems in a simpler way using low-cost chemicals in a quick manner.

From the energy consumption view point, the microwaves' processing has benefits with a lower carbon footprint. Figure 7 compares the energy required to process a feedstock of 1 t/h

1  
2  
3 of a CTAB-containing MCM-41, between calcination and microwaves. The calculation renders  
4  
5 a reduction of the energy consumption of 72%, from 149 down to 41 MW. Therefore, both  
6  
7 rapidness and energy reduction contribute to a more intensified process. These results are in  
8  
9 line with recent studies that have shown the benefit of microwave-assisted processing for  
10  
11 reactor operation under selective heating at both macro and microscale, whereas conven-  
12  
13 tional conduction heating is non-selective by itself or less efficient.<sup>48-50</sup>  
14  
15  
16  
17

## 18 **Conclusions**

20  
21 A rapidly-synthesised soft MCM-41 material was subjected to state-of-the-art thermal and  
22  
23 non-thermal SDA removal methods. Certain methods promoted severe hydrolysis and  
24  
25 provoked a collapse of the structure. Microwaves-assisted processing was effective and quick  
26  
27 in removing the SDA/surfactant and it yielded a different material than that obtained by  
28  
29 calcination. The hexagonal structure was preserved and broader pores were found, in addition  
30  
31 to the main ones; this was ascribed to some degree of hydrolysis, in combination with the  
32  
33 hydrothermal conditions during the microwave processing, but did not affect the total surface  
34  
35 area which was high. The surface of the material is highly rich in Si-OH, with a great promise  
36  
37 for further use. The benefits of the microwaves from the process point of view, as compared  
38  
39 to calcination, are the short processing time, that it is reduced from 14h (calcination) into 5  
40  
41 min (microwaves) and the lower applied temperature. The latter has an impact with a  
42  
43 reduction in 72% of the carbon footprint. This makes it appealing for further application to  
44  
45 other materials or other approaches, not necessarily oxidations but extractions.  
46  
47  
48  
49  
50  
51

## 52 **Associated content**

53  
54  
55 Supporting Information  
56  
57

1  
2  
3 The Supporting Information is available free of charge at X.  
4

5 Description of the chemicals employed for the synthesis and post-synthesis processing steps;  
6 elemental analyses of the processed materials; textural parameters of the processed materials  
7 (BET surface area, total pore volume, pore diameter and external surface area); scanning  
8 electron microscopy image of the synthesised mesophase; theoretical background for the  
9 energy balance calculation.  
10  
11  
12  
13  
14  
15  
16

## 17 **Conflict of interests**

18  
19  
20 There are no conflicts to declare.  
21  
22

## 23 **Acknowledgements**

24  
25  
26  
27 De Nederlandse Organisatie voor Wetenschappelijk Onderzoek (NWO, The Netherlands) is  
28 thanked for the financial support of the VIDI project no. 10284. L.L.P. thanks the UAM for grant  
29 number 22301055 (programa especial de la Dirección de Apoyo a la Investigación). O. Rojas  
30 and G. ten Brink (RUG) are thanked for assistance on the TEM images and preliminary results.  
31  
32  
33  
34  
35  
36  
37

## 38 **References**

- 39  
40  
41 (1) Zhao, D. Y.; Wan, Y.; Zhou, W. *Ordered Mesoporous Materials*; Wiley-VCH, Weinheim,  
42 2013.  
43  
44  
45 (2) Wang, Y.; Du, X.; Liu, Z.; Shi, S.; Lv, H. Dendritic fibrous nano-particles (DFNPs): rising  
46 stars of mesoporous materials, *J. Mater. Chem. A*, **2019**, *7*, 5111-5152  
47  
48  
49 (3) Wu, K. C.-W.; Jiang, X.; Yamauchi, Y. New trend on mesoporous films: precise controls  
50 of one-dimensional (1D) mesochannels toward innovative applications, *J. Mater.*  
51 *Chem.*, **2011**, *21*, 8934-8939.  
52  
53  
54  
55  
56  
57  
58  
59  
60

- 1  
2  
3 (4) IUPAC Gold Book, URL: <https://goldbook.iupac.org/terms/view/M03906>  
4  
5 (5) Parlett, C. M. A.; Wilson, K.; Lee, A. F. Hierarchical porous materials: catalytic  
6 applications, *Chem. Soc. Rev.*, **2013**, *42*, 3876-3893.  
7  
8  
9 (6) Zhao, D. Y. in *Introduction to Zeolite Science and Practice*, Vol. 168 (Eds: Cejka, J.; van  
10 Bekkum, H.; Corma, A.; Schüth, F.) 3<sup>rd</sup> revised Ed.; Elsevier B.V.: Amsterdam, 2007, p  
11 241-300.  
12  
13  
14  
15  
16 (7) Imhof, A.; Pine, D. J. Ordered macroporous materials by emulsion templating, *Nature*,  
17 **1997**, *389*, 948-951.  
18  
19  
20  
21 (8) Parlett, M. A.; Isaacs, M. A.; Beaumont, S. K.; Bingham, L. M.; Hondow, N. S.; Wilson,  
22 K.; Lee, A. F. Spatially orthogonal chemical functionalization of a hierarchical pore  
23 network for catalytic cascade reactions, *Nature Mater.* **2016**, *15*, 178-182.  
24  
25  
26  
27 (9) Kresge, T.; Leonowicz, M. E.; Roth, W. J.; Vartuli, J. C.; Beck, J. S. Ordered mesoporous  
28 molecular sieves synthesized by a liquid-crystal template mechanism, *Nature*, **1992**,  
29 *359*, 710-712.  
30  
31  
32  
33  
34 (10) López-Pérez, L.; Ortiz-Iniesta, M. J.; Zhang, Z.; Agirrezabal-Telleria, I.; Santes, M.;  
35 Heeres, H. J.; Melian-Cabrera, I. Detemplation of soft mesoporous silicananoparticles  
36 with structural preservation, *J. Mater. Chem. A*, **2013**, *1*, 4747- 4753.  
37  
38  
39  
40  
41 (11) Zhao, D. Y.; Feng, J.; Huo, Q.; Melosh, N.; Fredrickson, G. H.; Chmelka, B. F.; Stucky, G.  
42 D. Triblock copolymer syntheses of mesoporous silica with periodic 50 to 300 angstrom  
43 pores, *Science*, **1998**, *279*, 548-552.  
44  
45  
46  
47  
48 (12) Zhang, Z.; Melian-Cabrera, I. Modifying the hierarchical porosity of SBA-15 via mild-  
49 detemplation followed by secondary treatments, *J. Phys. Chem. C*, **2014**, *118*, 28689-  
50 28698.  
51  
52  
53  
54  
55  
56  
57  
58  
59  
60

- 1  
2  
3 (13) Huo, Q.; Margolese, D. I.; Ciesla, U.; Feng, P.; Gier, T. E.; Sieger, P.; Leon, R.; Petroff, P.  
4  
5 M.; Schüth, F.; Stucky, G. D. Generalized synthesis of periodic surfactant/inorganic  
6  
7 composite materials, *Nature*, **1994**, *368*, 317-321.  
8  
9  
10 (14) Alfredsson, V.; Anderson, M. W. Structure of MCM-48 revealed by transmission  
11  
12 electron microscopy, *Chem. Mater.*, **1996**, *8*, 1141-1146.  
13  
14 (15) Liu, X.; Tian, B.; Yu, C.; Gao, F.; Xie, S.; Tu, B.; Che, R.; Peng, L-M.; Zhao, D. Y.  
15  
16 Room-temperature synthesis in acidic media of large-pore three-dimensional  
17  
18 bicontinuous mesoporous silica with *la3d* symmetry, *Angew. Chem. Int. Ed.*, **2002**, *41*,  
19  
20 3876-3878.  
21  
22  
23 (16) Gao, C.; Sakamoto, Y.; Sakamoto, K.; Terasaki, O.; Che, S. Synthesis and  
24  
25 characterization of mesoporous silica AMS-10 with bicontinuous cubic *Pn<sub>3</sub>m*  
26  
27 symmetry, *Angew. Chem. Int. Ed.*, **2006**, *45*, 4295-4298.  
28  
29  
30 (17) Huo, Q.; Leon, R.; Petroff, P. M.; Stucky, G. D. Mesostructure design with gemini  
31  
32 surfactants: supercage formation in a three-dimensional hexagonal array, *Science*,  
33  
34 **1995**, *268*, 1324-1327.  
35  
36  
37 (18) Yu, C. Z.; Yu, Y. H.; Miao, L.; Zhao, D. Y. Highly ordered mesoporous silica structures  
38  
39 templated by poly(butylene oxide) segment di- and tri-block copolymers, *Micropor.*  
40  
41 *Mesopor. Mat.*, **2001**, *44-45*, 65-72.  
42  
43  
44 (19) Zhao, D. Y.; Huo, Q. S.; Feng, J. L.; Kim, J. M.; Han, Y. J.; Stucky, G. D. Novel mesoporous  
45  
46 silicates with two-dimensional mesostructure direction using rigid bolaform  
47  
48 surfactants, *Chem. Mater.*, **1999**, *11*, 2668-2672.  
49  
50  
51 (20) Kimura, T.; Kamata, T.; Fuziwara, M.; Takano, Y.; Kaneda, M.; Sakamoto, Y.; Terasaki,  
52  
53 O.; Sugahara, Y.; Kuroda, K. Formation of novel ordered mesoporous silicas with square  
54  
55  
56  
57  
58  
59  
60

- 1  
2  
3 channels and their direct observation by transmission electron microscopy, *Angew.*  
4  
5 *Chem. Int. Ed.*, **2000**, *39*, 3855-3859.  
6  
7 (21) Ryoo, R.; Kim, J. M.; Ko, C. H.; Shin, C. H. Disordered molecular sieve with branched  
8  
9 mesoporous channel network, *J. Phys. Chem.*, **1996**, *100*, 17718-17721.  
10  
11 (22) Tanev, P. T.; Pinnavaia, T. J. Mesoporous silica molecular sieves prepared by ionic and  
12  
13 neutral surfactant templating: a comparison of physical properties, *Chem. Mater.*,  
14  
15 **1996**, *8*, 2068-2079.  
16  
17 (23) Kleitz, F.; Liu, D. N.; Anilkumar, G. M.; Park, I. S.; Solovyov, L. A.; Shmakov, A. N.; Ryoo,  
18  
19 R. Large cage face-centered-Cubic *Fm3m* mesoporous silica: synthesis and structure,  
20  
21 *J. Phys. Chem. B*, **2003**, *107*, 14296-14300.  
22  
23 (24) Bagshaw, S. A.; Prouzet, E.; Pinnavaia, T. J. Templating of mesoporous molecular sieves  
24  
25 by nonionic polyethylene oxide surfactants, *Science*, **1995**, *269*, 1242-1244.  
26  
27 (25) Bagshaw, S. A.; Pinnavaia, T. J. Mesoporous alumina molecular sieves, *Angew. Chem.*  
28  
29 *Int. Ed.*, **1996**, *35*, 1102-1105.  
30  
31 (26) López-Pérez, L.; Perdriau, S.; ten Brink, G.; Kooi, B. J.; Heeres, H. J.; Melián-Cabrera, I.  
32  
33 Stabilization of self-assembled alumina mesophases, *Chem. Mater.*, **2013**, *25*, 848-855.  
34  
35 (27) López-Pérez, L.; Alvarez-Galván, C.; Zarubina, V.; Figueiredo Fernandes, B. O.; Melián-  
36  
37 Cabrera, I. A hydrothermally stable transition alumina by condensation-enhanced self-  
38  
39 assembly and pyrolysis crystallization: application in the steam reforming of methane,  
40  
41 *Cryst. Eng. Comm.*, **2014**, *16*, 6775-6783.  
42  
43 (28) Xu, R.; Pang, W. Q.; Yu, J. H.; Huo, Q. H.; Chen, J. H. *Chemistry of Zeolites and Related*  
44  
45 *Porous Materials: Synthesis and Structure*; John Wiley & Sons: Singapore, 2007.  
46  
47  
48  
49  
50  
51  
52  
53  
54  
55  
56  
57  
58  
59  
60

- 1  
2  
3 (29) Leng, Y.; Liu, J.; Zhang, Z.; Chen, H.; Zhang, P.; Dai, S. Polyoxometalates as bifunctional  
4 templates: engineering metal oxides with mesopores and reactive surfaces for  
5 catalysis, *J. Mater. Chem. A*, **2019**, *7*, 27297-27303.  
6  
7  
8  
9  
10 (30) Weng, Z.; Chen, Z.; Qin, X.; Zaera, F. Sub-monolayer control of the growth of oxide films  
11 on mesoporous materials, *J. Mater. Chem. A*, **2018**, *6*, 17548-17558.  
12  
13  
14 (31) López Pérez, L.; Ortiz-Iniesta, M. J.; Heeres, H. J.; Melián-Cabrera, I. Hot-spots during  
15 the calcination of MCM-41: A SAXS comparative analysis of a soft mesophase, *Mater.*  
16 *Lett.* **2014**, *118*, 51-54.  
17  
18  
19  
20  
21 (32) Schüth, F.; Sing, K. S. W.; Weitkamp, J. (Eds.), Handbook of Porous Solids; Wiley-VCH:  
22 Weinheim, 2002; pp. 1546-1551.  
23  
24  
25  
26 (33) Zhang, Z.; Yin, J.; Heeres, H. J.; Melián-Cabrera, I. Thermal detemplation of SBA-15  
27 mesophases. Effect of the activation protocol on the framework contraction, *Micropor.*  
28 *Mesopor. Mat.*, **2013**, *176*, 103-111.  
29  
30  
31  
32  
33 (34) Patarin, J. Mild methods for removing organic templates from inorganic host materials,  
34 *Angew. Chem. Int. Ed.*, **2004**, *43*, 3878-3880.  
35  
36  
37  
38 (35) González-Rivera, J.; Tovar-Rodríguez, J.; Bramanti, E.; Duce, C.; Longo, I.; Fratini, E.;  
39 Galindo-Esquivel, I. R.; Ferrari, C. Surfactant recovery from mesoporous metal-  
40 modified materials (Sn-, Y-, Ce-, Si-MCM-41), by ultrasound assisted ion-exchange  
41 extraction and its re-use for a microwave in situ cheap and eco-friendly MCM-41  
42 synthesis, *J. Mater. Chem. A*, **2014**, *2*, 7020-7033.  
43  
44  
45  
46  
47  
48 (36) Grün, M.; Unger, K. K.; Matsumoto, A. Novel pathways for the preparation of  
49 mesoporous MCM-41 materials: control of porosity and morphology, *Micropor.*  
50 *Mesopor. Mat.*, **1999**, *27*, 207-216.  
51  
52  
53  
54  
55  
56  
57  
58  
59  
60

- 1  
2  
3 (37) Tian, B.; Liu, X.; Yu, C.; Gao, F.; Luo, Q.; Xie, S.; Tu, B.; Zhao, D. Y. Microwave assisted  
4 template removal of siliceous porous materials, *Chem. Commun.*, **2002**, 1186-1187.  
5  
6  
7 (38) Büchel, G.; Denoyel, R.; Llewellyn, P. L.; Rouquerol, J. In situ surfactant removal from  
8 MCM-type mesostructures by ozone treatment, *J. Mater. Chem.*, **2001**, *11*, 589-593.  
9  
10  
11  
12 (39) Kleitz, F.; Schmidt, W.; Schüth, F. Evolution of mesoporous materials during the  
13 calcination process: structural and chemical behavior, *Micropor. Mesopor. Mat.*, **2001**,  
14 *44-45*, 95-109.  
15  
16  
17  
18 (40) Kleitz, F.; Schmidt, W.; Schüth, F. Calcination behavior of different surfactant-  
19 templated mesostructured silica materials, *Micropor. Mesopor. Mat.*, **2003**, *65*, 1-29.  
20  
21  
22  
23 (41) Groen, J. C.; Pérez-Ramírez, J. Critical appraisal of mesopore characterization by  
24 adsorption analysis, *Appl. Catal. A*, **2004**, *268*, 121-125.  
25  
26  
27  
28 (42) Lowell, S.; Shields, J. E.; Thomas, M. A.; Thommes, M. Characterization of Porous Solids  
29 and Powders: Surface Area, Pore Size and Density; Springer: Dordrecht, 2004.  
30  
31  
32  
33 (43) Fubini, B.; Bolis, V.; Cavenago, A.; Garrone, E.; Ugliengo, P. Structural and induced  
34 heterogeneity at the surface of some silica polymorphs from the enthalpy of  
35 adsorption of various molecules, *Langmuir*, **1993**, *9*, 2712-2720.  
36  
37  
38  
39 (44) Majda, D.; Zimowska, M.; Tarach, K.; Góra-Marek, K.; Napruszewska, B. D.; Michalik-  
40 Zym, A. Water thermoporosimetry as a tool of characterization of the textural  
41 parameters of mesoporous materials, *J. Therm. Anal. Calorim.*, **2017**, *127*, 207-220.  
42  
43  
44  
45 (45) Zhang, Z.; Santangelo, D. L.; ten Brink, G.; Kooi, B. J.; Moulijn, J. A.; Melián-Cabrera, I.  
46 On the drug adsorption capacity of SBA-15 obtained from various detemplation  
47 protocols, *Mater. Lett.* **2014**, *131*, 186–189.  
48  
49  
50  
51  
52 (46) Lide, D. R. CRC Handbook of Chemistry and Physics, 89<sup>th</sup> Ed.; CRC Press Taylor Francis  
53 Group: Boca Raton, 2008; p 8-20.  
54  
55  
56  
57  
58  
59  
60

- 1  
2  
3 (47) Tarr, M. A. *Chemical Degradation Methods for Wastes and Pollutants: Environmental*  
4 *and Industrial Applications*; Marcel Dekker, Inc.: New York, 2003; p 5.  
5  
6  
7 (48) Xiouras, C.; Radacsi, N.; Sturm, G.; Stefanidis, G. D. Furfural synthesis from d-xylose in  
8 the presence of sodium chloride: microwave versus conventional heating, *Chem. Sus.*  
9 *Chem.*, **2016**, *9*, 2159-2166.  
10  
11  
12  
13  
14 (49) Priecel, P.; Lopez-Sanchez, J. A. Advantages and limitations of microwave reactors:  
15 from chemical synthesis to the catalytic valorization of biobased chemicals, *ACS*  
16 *Sustain. Chem. Eng.*, **2019**, *7*, 3-21.  
17  
18  
19  
20  
21 (50) Navarro, M.; Morris, S. A.; Mayoral, A.; Cejka, J.; Morris, R. E. Microwave heating and  
22 the fast ADOR process for preparing zeolites, *J. Mater. Chem. A*, **2017**, *5*, 8037–8043.  
23  
24  
25  
26  
27  
28  
29  
30  
31  
32  
33  
34  
35  
36  
37  
38  
39  
40  
41  
42  
43  
44  
45  
46  
47  
48  
49  
50  
51  
52  
53  
54  
55  
56  
57  
58  
59  
60

**Table 1.** MCM-41 materials' properties after applying various SDA removal methodologies.

Material	SDA removal (%) <sup>(a)</sup>	$a_0$ (nm) <sup>(b)</sup>	$S_{\text{BET}}$ (m <sup>2</sup> /g)	$V_{\text{total}}$ (cm <sup>3</sup> /g)
Mesophase (untreated)	0 (reference)	4.76	21	0.04
Calcination	100	4.28	1077	0.85
Solvent extraction	97	Am <sup>(c)</sup>	456	0.25
Ozone	29	4.57	545	0.31
Microwaves	99	4.49	923	0.82
Fenton	98	4.68	636	0.37

<sup>(a)</sup> SDA removal calculated as:  $\eta(\%) = \left(1 - \frac{C^{\text{material}}}{C^{\text{mesophase}}}\right) \times 100$ , where  $C^{\text{material}}$  is the carbon concentration of the material and  $C^{\text{mesophase}}$  is the carbon concentration of the mesophase; the raw data (wt % C) can be found in the ESI, Table S2.

<sup>(b)</sup>  $a_0$  = the lattice parameter, from the SAXS pattern:  $a_0 = (2/\sqrt{3}) \cdot d_{100}$ .

<sup>(c)</sup> fully amorphous.

**Table 2.** Quantification of the  $^{29}\text{Si}$  MAS NMR  $Q_n$  species and Si-OH concentration.

Material	$Q_2$ (%)	$Q_3$ (%)	$Q_4$ (%)	Si-OH (%) <sup>(a,b)</sup>
Mesophase (untreated)	0.5	37.7	61.8	38.7 (100)
Calcination	0.7	30.1	69.2	31.5 (81)
Microwaves	2.1	33.4	64.5	37.6 (97)

$$^{(a)} \text{Si-OH}(\%) = \left[ \frac{2Q_2 + Q_3}{\sum Q_i} \right] \times 100.$$

<sup>(b)</sup> Value between parenthesis corresponds to the percentage of retention of the Si-OH using the parent mesophase as reference (*i.e.* 100%).

**Table 3.** Comparison of the various SDA removal methodologies.

Methodology	Material's features		
	SDA removal	Ordering	Porosity
Calcination	++	++	++
Solvent extraction	++	–	<500 m <sup>2</sup> /g, flat PSD
Ozone	+	–	<600 m <sup>2</sup> /g, flat PSD
Microwaves	++	+	++ with some pore expansion
Fenton	++	+/-	<650 m <sup>2</sup> /g, flat PSD

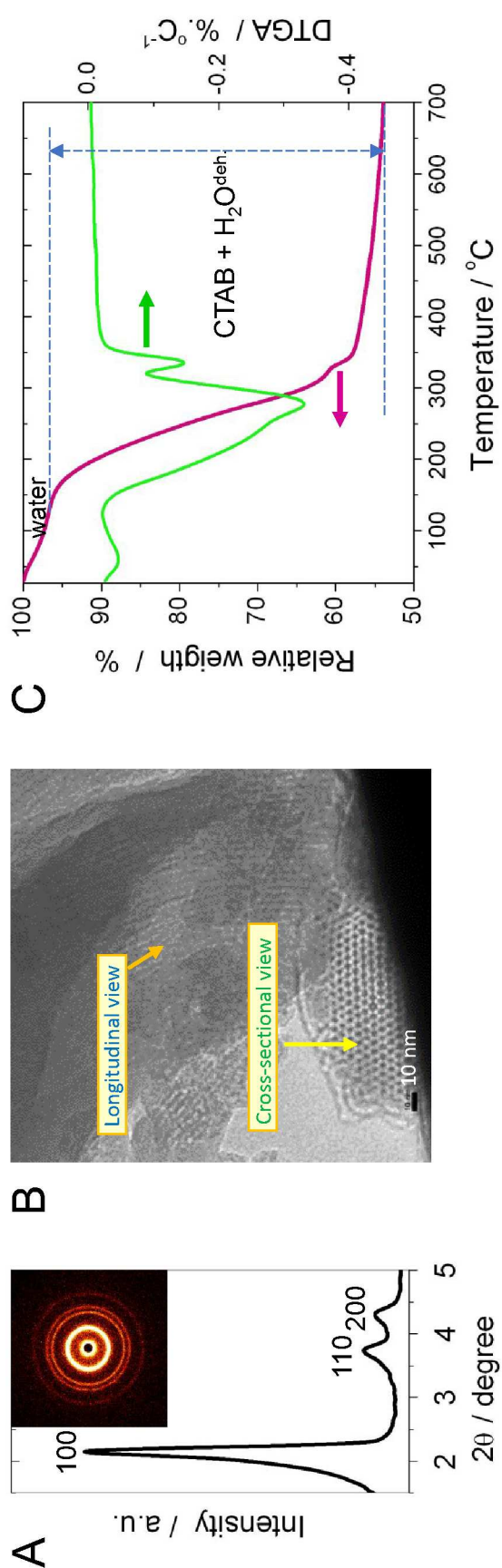


**Figure 1.** MCM-41 mesophase. **A**) SAXS (inset: measured 2D scattering pattern), **B**) high-resolution TEM and **C**) TGA/DTGA analyses. In **C**)

CTAB+ $\text{H}_2\text{O}^{\text{deh.}}$ . means that the weight loss is due to the combustion of the CTAB plus the water coming from the dehydroxylation of the material

( $2\text{Si-OH} \rightarrow \text{Si-O-Si} + \text{H}_2\text{O}$ ); that is the reason we employed CHN elemental analysis, as it is an element-selective technique.

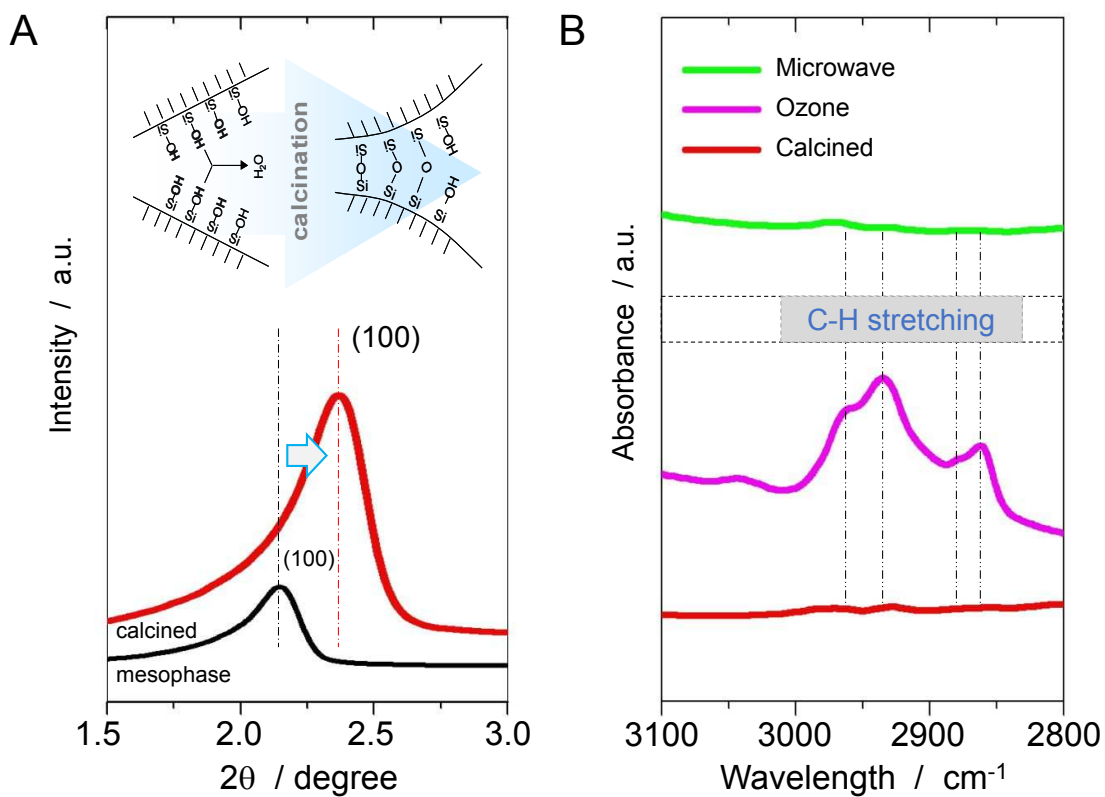


**Figure 2.** A) SAXS patterns in the (001) region of the mesophase and calcined counterpart. Inset: representation of the structural shrinkage upon calcination. Silanol groups combine and siloxane bonds are formed, resulting in structural shrinkage with a loss of pore volume. B) DRIFTS spectra of the C-H region for three relevant materials.

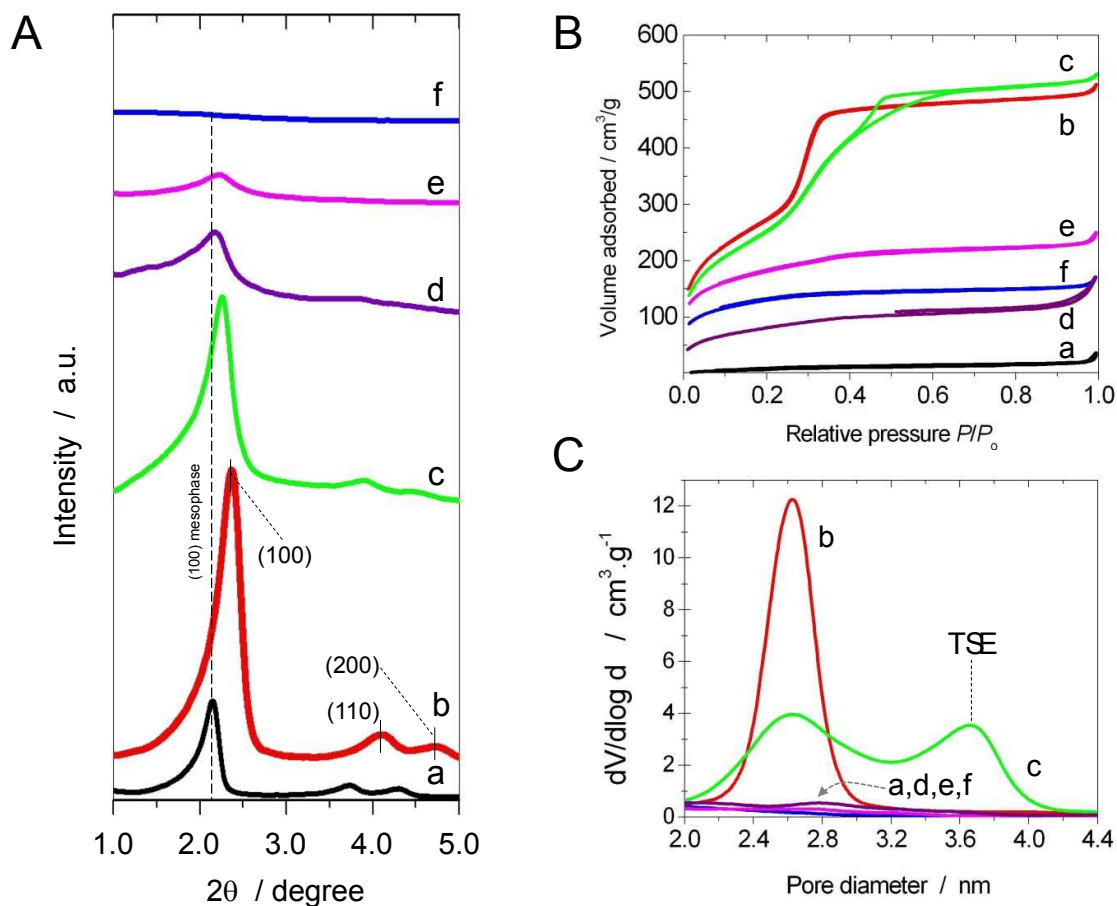


**Figure 3.** Effect of the SDA removal methodologies on the MCM-41. **A)** SAXS patterns. **B)**  $N_2$  adsorption isotherms. **C)** BJH pore-size distribution. Materials: **a)** untreated mesophase, **b)** calcination, **c)** microwaves, **d)** Fenton chemistry, **e)** ozonation and **f)** solvent extraction. Isotherms in **B** were offset for clarity.

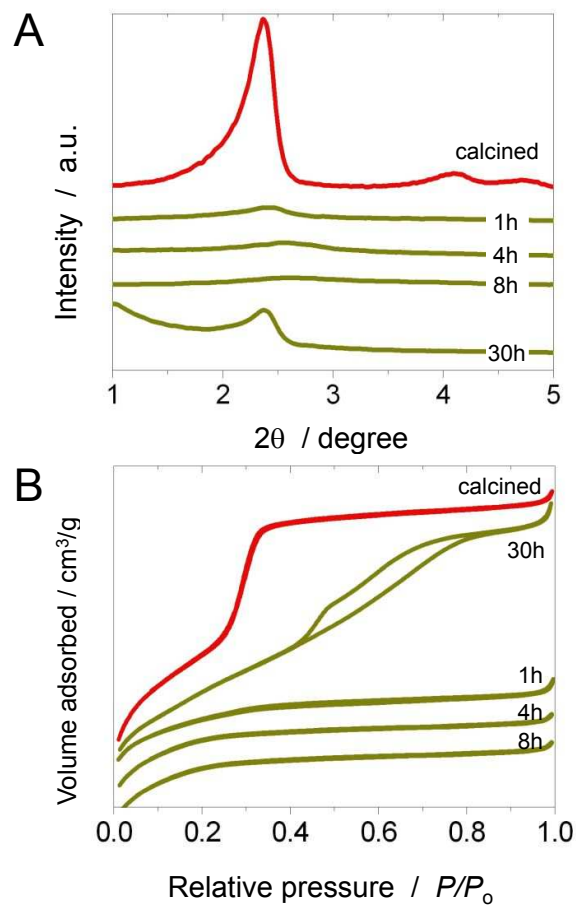


**Figure 4.** Stability of the MCM-41 after hydrothermal treatment at 70 °C. **A)** Evolution of the structural changes by SAXS, treatment time is indicated. **B)** Nitrogen sorption isotherms of the corresponding materials.

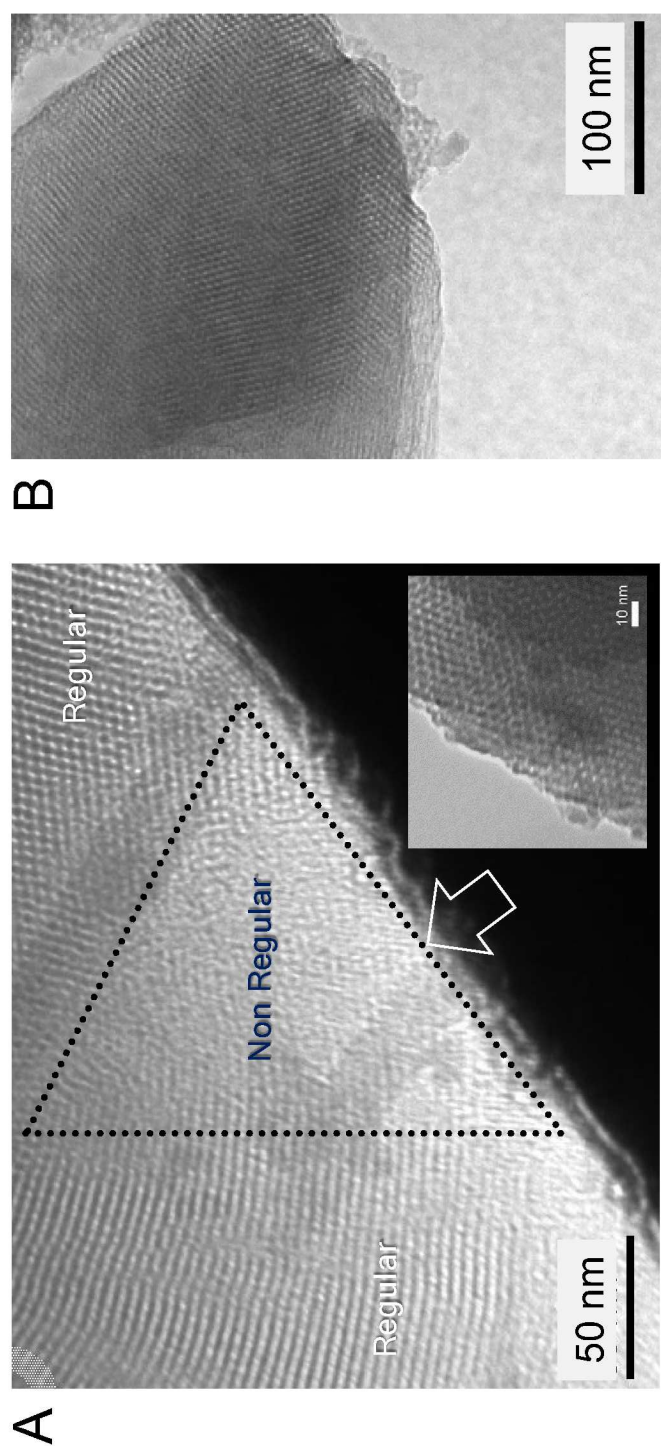


**Figure 5.** A) High-resolution TEM of the microwaved-processed structure showing areas with damage associated to hydrolysis (highlighted with arrow). The inset shows a front view of the pores having a well-defined hexagonal symmetry. B) High-resolution TEM of the calcined material.

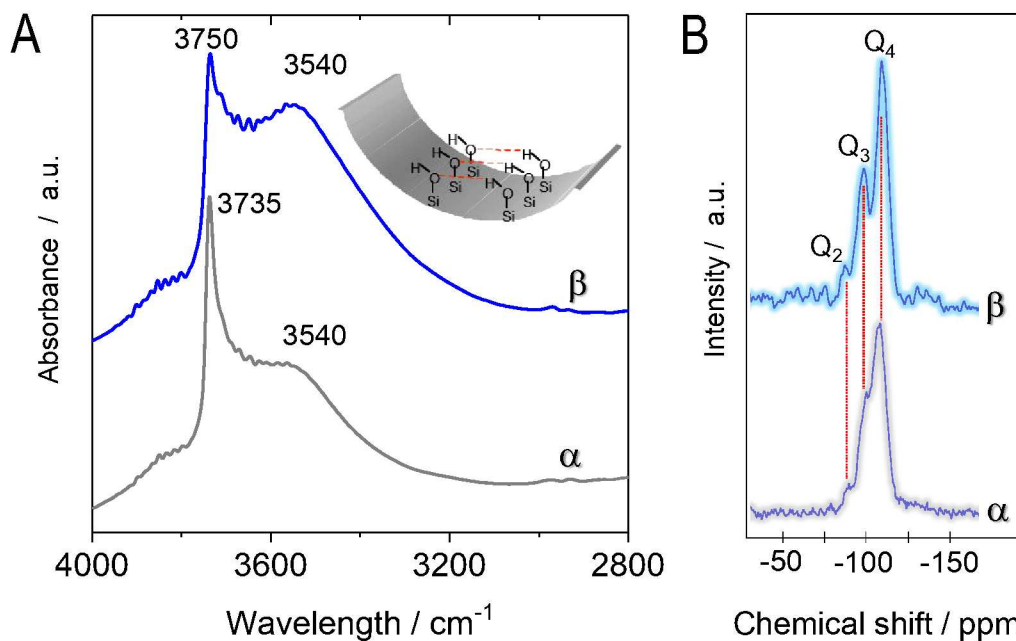


**Figure 6.** A) DRIFTS analysis of the O-H region; the inset represents a highly hydroxylated surface in the microwaved material's surface. B) <sup>29</sup>Si MAS NMR spectra. Materials:  $\alpha$ ) calcined and  $\beta$ ) microwaved-processed materials.

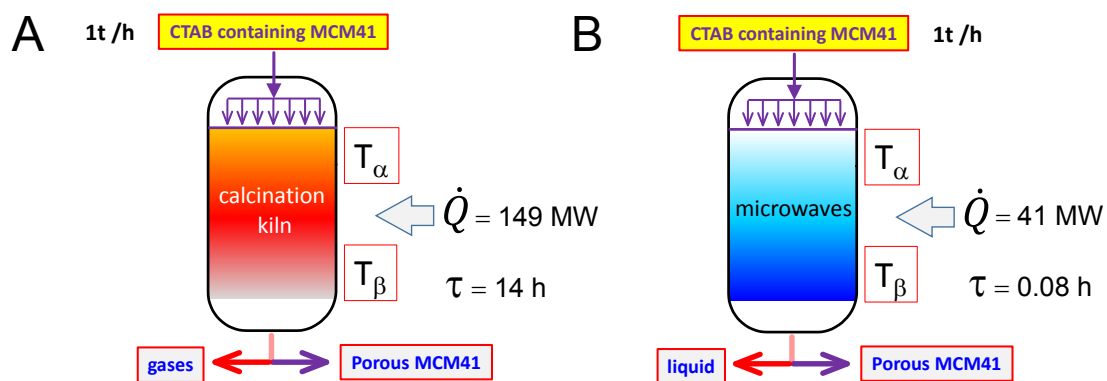


**Figure 7.** Reactor models representing calcination (A) and the microwaves-processing (B) of a solid feedstock of 1 t/h of CTAB-containing MCM-41. The methodology can be found in the Electronic Supporting Information.